

Extrinsic Calibration of Non-overlapping Camera-Laser System using Structured Environment

Yunsu Bok, Dong-Geol Choi, Pascal Vasseur and In So Kweon

Abstract—In this paper are presented simple and practical solutions to extrinsic calibration between a camera and a 2D laser sensor, without overlap. Previous methods utilized a plane or an intersecting line of two planes as a geometric constraint with enough common field-of-view. These required additional sensors to calibrate non-overlapping systems. In this paper, we present two methods for solving the problem – one utilizes a plane; the other utilizes an intersecting line of two planes. For each method, an initial solution of the relative positions of a non-overlapping camera and a laser sensor, was computed by adopting a reasonable assumption about geometric structures. Then we refined it via non-linear optimization, even if the assumption was not perfectly satisfied. Both simulation results and experiments using real data showed that the proposed methods provided reliable results compared to ground-truth, and similar or better results than those provided by a conventional method.

I. INTRODUCTION

Cameras and range sensors are the most popular sensors for robotic applications. They provide projected images and depth (distance) information in their field of view, and various applications using them have been researched for many decades. Camera-based methods have been developed in the research area of computer vision rather than in robotics. SFM(structure from motion) attempts to estimate the poses of cameras and to reconstruct 3D structures in large-scale environments [1], [2]. Core algorithms and applications of visual SLAM(simultaneous localization and mapping) in 3D space [3] are being developed by many researchers. Range-sensor-based methods are being developed for robotics. SLAM in indoor environments using a 2D laser sensor is a traditional issue [4] and is still being researched. Two-dimensional laser sensors are also used to reconstruct 3D structures in outdoor scenes [5], [6], [7]. Three-dimensional laser sensors are powerful for use in 3D reconstruction [8], but they were not popular until a few years ago because of their high cost. In recent years, several types of 3D range sensors (e.g., time-of-flight cameras, Velodyne and Kinect) have become popular.

Cameras and range sensors have different characteristics, and their fusion complements the weaknesses of both sensors. Fusion of cameras and 2D laser sensors are used for localization [9], [10], [11] and mapping [12], [13]. Kinect

can be classified as a fusion system because it provides both images and range data. A number of studies related to geometry [14], [15], [16] and photometry [17], [18], [19] used Kinect as the main sensor.

Extrinsic calibration of sensor systems is essential for utilizing data from various sensors in a single framework. Extrinsic calibration of multiple-camera systems is a traditional issue in this area of research. The relative pose between non-overlapping cameras is computed by estimating the motion of each camera and solving the $AX=XB$ problem [28], or by other methods [20], [21]. Calibration of cameras and 3D range sensors can be solved in the same way, or by using geometric constraints of the objects scanned by them [22], [23]. Recently, Choi *et al.* [29] proposed a calibration method of two, 2D laser sensors.

This paper is focused on extrinsic calibration of a camera with a 2D laser sensor. The first solution to this problem was proposed by Zhang and Pless [24]. The solution minimized the Euclidean distance between a planar pattern and scan data. Mei and Rives [25] used similar geometric constraint for extrinsic calibration. Li *et al.* [26] and Bok *et al.* [13] proposed line-feature-based algorithms. All of them require adequate overlap between a camera and a 2D laser sensor.

For applications such as robots and ground vehicles, sensors have different heading directions depending on their individual purposes. In this paper, we present practical solutions for extrinsic calibration of a camera and a 2D laser sensor ‘without overlap’. Until now, this problem could be solved indirectly by attaching an additional camera with overlap and then estimating two relative poses: between the laser sensor and the additional camera with overlap, and between the two cameras. Direct calibration between non-overlapping sensors is important because it does not require any bridging sensor (camera in this case) and it can be utilized as an additional constraint for system calibration, even if the system can also be calibrated using conventional methods. To our knowledge, this work is the first attempt to solve the problem.

We present two methods which utilize reasonable assumptions about geometric features such as a plane or an intersecting line of two planes. For each method, we obtain an initial solution via SVD(singular value decomposition). This is then refined via non-linear optimization, which does not require any assumption about structures but estimates the parameters of geometric features. Both simulation results and experiments using real data provided reliable results, compared to ground-truth.

Y. Bok is a research assistant professor of Division of Future Vehicle, KAIST, Korea ysbok@rcv.kaist.ac.kr

D.-G. Choi is a Ph.D. student of the Robotics Program, KAIST, Korea dgchoi@rcv.kaist.ac.kr

P. Vasseur is with Laboratory LITIS, Université de Rouen, France pascal.vasseur@univ-rouen.fr

I. S. Kweon (corresponding author) is a professor of Department of Electrical Engineering, KAIST, Korea iskweon@kaist.ac.kr

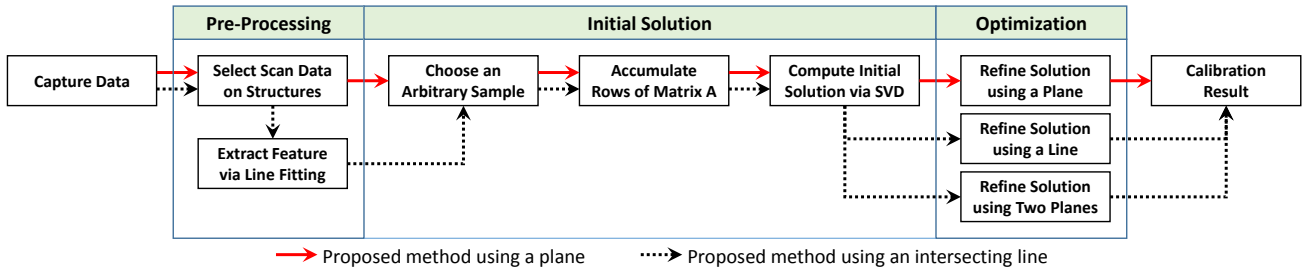


Fig. 1. Flow chart of the proposed method

II. OVERVIEW OF PROPOSED METHODS

A flow chart of the proposed methods is shown in Fig. 1. It contains one method using a plane, and another using an intersecting line of two planes. First, we captured images and scanned data simultaneously while a camera viewed a planar pattern and a 2D laser sensor scanned a user-defined structure. A relative pose between the structure and the planar pattern must be fixed and close to an assumption, which will be explained in Sect. III. Assuming that the camera is calibrated, a relative pose between the camera and the planar pattern may be computed easily. Then we manually selected a part of the scan data that overlapped the structure. This approach is widely used in system calibration, except for self-calibration. An example of data selection is shown in Fig. 3(a). If we want to utilize an intersecting line, we extract a feature from the scan data via line fitting. From among the selected data, we chose an arbitrary sample and then accumulated rows of matrix \mathbf{A} using the sample (see Sect. III). The singular vector of the matrix \mathbf{A} corresponding to the minimum singular value, is an initial solution of the relative pose between the sensors. Finally, this is refined via non-linear optimization whose cost-function depends on structures. The cost function for each method is designed to minimize the sum of geometric errors (see Sect. IV).

III. SOLVING NON-OVERLAPPING SYSTEM

In this paper, a coordinate system of a planar pattern was set to a ‘world coordinate system’. A pose of the planar pattern is defined as $z = 0$. We compute intrinsic parameters of a camera and a relative pose between the camera and the planar pattern using a conventional camera calibration method. Let $[\mathbf{R}_{CW} \ \mathbf{t}_{CW}]$ be a known transformation from camera coordinate to world coordinate (i.e., inverse of projection matrix).

The scanning plane of a 2D laser sensor was set equal to $y = 0$ in a laser coordinate system. A scanned point with distance d and angle θ was converted into a Cartesian point $\mathbf{q}_L = [x_L \ 0 \ z_L]^T$ in the laser coordinate system using (1). Adopting an unknown transformation $[\mathbf{R}_{LC} \ \mathbf{t}_{LC}]$ from laser coordinate to camera coordinate, a point was transformed into a world coordinate system $\mathbf{q}_W = [x_W \ y_W \ z_W]^T$, as shown in Equation 2.

$$\mathbf{q}_L = \begin{bmatrix} x_L \\ 0 \\ z_L \end{bmatrix} = \begin{bmatrix} d \cos \theta \\ 0 \\ d \sin \theta \end{bmatrix} \quad (1)$$

$$\mathbf{q}_W = [\mathbf{R}_{CW} \ \mathbf{t}_{CW}] \begin{bmatrix} \mathbf{R}_{LC} & \mathbf{t}_{LC} \\ \mathbf{0}^T & 1 \end{bmatrix} \begin{bmatrix} \mathbf{q}_L \\ 1 \end{bmatrix} \quad (2)$$

The laser-to-world transformation (2) is simplified to $\mathbf{q}_W = \mathbf{H}\mathbf{q}_L$ in the rest of this paper.

Let R_{ij} and r_{ij} be the elements of \mathbf{R}_{LC} and \mathbf{R}_{CW} at i -th row and j -th column, and T_i and t_i be i -th elements of \mathbf{t}_{LC} and \mathbf{t}_{CW} , respectively. In (3), x_W , y_W and z_W are expressed by multiplication of known 10×1 vectors \mathbf{v}_x , \mathbf{v}_y , \mathbf{v}_z and an unknown 10×1 vector \mathbf{x} , respectively. An initial solution of $[\mathbf{R}_{LC} \ \mathbf{t}_{LC}]$ was computed using (3).

In this section, we provide two methods: one using a plane and another using an intersecting line of two planes.

$$\mathbf{q}_W = \begin{bmatrix} x_W \\ y_W \\ z_W \end{bmatrix} = [\mathbf{v}_x \ \mathbf{v}_y \ \mathbf{v}_z]^T \mathbf{x} \quad (3)$$

$$[\mathbf{v}_x \ \mathbf{v}_y \ \mathbf{v}_z] = \begin{bmatrix} r_{11}x_L & r_{21}x_L & r_{31}x_L \\ r_{11}z_L & r_{21}z_L & r_{31}z_L \\ r_{12}x_L & r_{22}x_L & r_{32}x_L \\ r_{12}z_L & r_{22}z_L & r_{32}z_L \\ r_{13}x_L & r_{23}x_L & r_{33}x_L \\ r_{13}z_L & r_{23}z_L & r_{33}z_L \\ r_{13} & r_{23} & r_{33} \\ t_1 & t_2 & t_3 \end{bmatrix}, \ \mathbf{x} = \begin{bmatrix} R_{11} \\ R_{13} \\ T_1 \\ R_{21} \\ R_{23} \\ T_2 \\ R_{31} \\ R_{33} \\ T_3 \\ 1 \end{bmatrix} \quad (4)$$

A. Solution Using a Plane

The first solution for camera-laser calibration is to utilize a plane. This is similar to the method proposed by Zhang and Pless [24]. One difference between them is that we do not know a pose of the plane. Instead, we just assume that the plane is perpendicular to one of the axes of the world coordinate system (i.e., coordinate system of a planar pattern). An example of scanning a plane perpendicular to the x -axis is shown in Fig. 2(a).

For example, let us assume that the plane is perpendicular to a y -axis of the world coordinate system. A floor or ceiling with a vertical planar pattern is an example of this

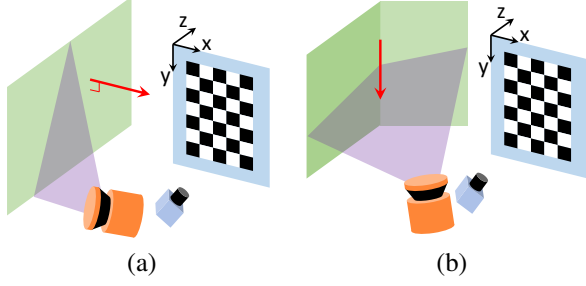


Fig. 2. Examples of assumptions about structures: (a) A plane whose normal vector (red arrow) is parallel to the x-axis of the world coordinate system, (b) An intersecting line (red arrow) of two planes parallel to the y-axis of the world coordinate system. The two planes do not have to be perpendicular to any axis.

configuration. The plane is expressed by $y = K$ with an unknown constant K . We cannot solve $y_W = \mathbf{v}_y^\top \mathbf{x} = K$ without an exact value of K . Using an arbitrary point $\mathbf{q}'_L = [x'_L \ 0 \ z'_L]^\top$ selected from a frame with camera-to-world transformation $[\mathbf{R}'_{CW} \ \mathbf{t}'_{CW}]$, the point-plane constraint (the scanned point must lie on the plane) is changed into a new constraint – scanned points must have the same (unknown) distance from the plane – which can be expressed in the form $\mathbf{A}\mathbf{x} = 0$.

$$(\mathbf{v}_y - \mathbf{v}'_y)^\top \mathbf{x} = \begin{bmatrix} r_{21}x_L - r'_{21}x'_L \\ r_{21}z_L - r'_{21}z'_L \\ r_{21} - r'_{21} \\ r_{22}x_L - r'_{22}x'_L \\ r_{22}z_L - r'_{22}z'_L \\ r_{22} - r'_{22} \\ r_{23}x_L - r'_{23}x'_L \\ r_{23}z_L - r'_{23}z'_L \\ r_{23} - r'_{23} \\ t_2 - t'_2 \end{bmatrix}^\top \begin{bmatrix} R_{11} \\ R_{13} \\ T_1 \\ R_{21} \\ R_{23} \\ T_2 \\ R_{31} \\ R_{33} \\ T_3 \\ 1 \end{bmatrix} = 0 \quad (5)$$

Theoretically only two points are valid for each frame, because they define a line on which the other points lie. In order to obtain a unique solution, at least five frames must be captured in different poses. Equation (5) can be modified to (6) or (7), using (4), if the plane is perpendicular to the x- or z-axis of the world coordinate system, respectively.

$$(\mathbf{v}_x - \mathbf{v}'_x)^\top \mathbf{x} = 0 \quad (6)$$

$$(\mathbf{v}_z - \mathbf{v}'_z)^\top \mathbf{x} = 0 \quad (7)$$

B. Solution Using an Intersecting Line

The second solution to camera-laser calibration is to utilize an intersecting line of two planes. Similar to Sect. III-A, we assumed that an intersecting line is parallel to one axis of the world coordinate system. An example of scanning an intersecting line parallel to the y-axis is shown in Fig. 2(b). Planes which intersect at the line do not have to be perpendicular to each other or to an axis of the world coordinate system. In this case, we did not use all of scan data to compute an initial solution. Instead, we extracted a feature point on the line for each scan (see Fig. 3(b)). Two

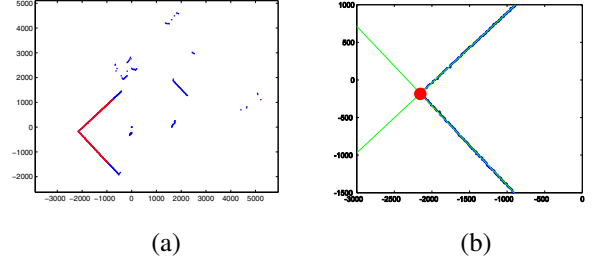


Fig. 3. An example of feature extraction from scan data. (a) A part of scan data (red) on two planes is selected manually. (b) An intersection of two fitted lines (green lines) are extracted as a feature point (red dot).

lines were extracted from scan data on two planes via line fitting, and their intersection was considered the feature-point $\hat{\mathbf{q}}_L = [\hat{x}_L \ 0 \ \hat{z}_L]^\top$ of the frame.

For example, let us assume that an intersecting line is parallel to the y-axis of the world coordinate system. A corner of the indoor environment with a vertical planar pattern is an example of this configuration. The line is expressed by $x = K_1$ and $z = K_2$ with unknown constants K_1 and K_2 . Similar to Sect. III-A, an arbitrary frame was selected and the other frames were used to generate a matrix of form $\mathbf{A}\mathbf{x} = 0$.

Let $\hat{\mathbf{q}}'_L = [\hat{x}'_L \ 0 \ \hat{z}'_L]^\top$ and $[\mathbf{R}'_{CW} \ \mathbf{t}'_{CW}]$ be a feature point, respectively. The point-line constraint (feature point must lie on line) is also changed into a new constraint – feature points must have the same (unknown) x- and z-coordinates in the world coordinate system – which can be expressed in the form $\mathbf{A}\mathbf{x} = 0$.

$$[\hat{\mathbf{v}}_x - \hat{\mathbf{v}}'_x \ \hat{\mathbf{v}}_z - \hat{\mathbf{v}}'_z]^\top \mathbf{x} = \begin{bmatrix} r_{11}\hat{x}_L - r'_{11}\hat{x}'_L & r_{31}\hat{x}_L - r'_{31}\hat{x}'_L \\ r_{11}\hat{z}_L - r'_{11}\hat{z}'_L & r_{31}\hat{z}_L - r'_{31}\hat{z}'_L \\ r_{11} - r'_{11} & r_{31} - r'_{31} \\ r_{12}\hat{x}_L - r'_{12}\hat{x}'_L & r_{32}\hat{x}_L - r'_{32}\hat{x}'_L \\ r_{12}\hat{z}_L - r'_{12}\hat{z}'_L & r_{32}\hat{z}_L - r'_{32}\hat{z}'_L \\ r_{12} - r'_{12} & r_{32} - r'_{32} \\ r_{13}\hat{x}_L - r'_{13}\hat{x}'_L & r_{33}\hat{x}_L - r'_{33}\hat{x}'_L \\ r_{13}\hat{z}_L - r'_{13}\hat{z}'_L & r_{33}\hat{z}_L - r'_{33}\hat{z}'_L \\ r_{13} - r'_{13} & r_{33} - r'_{33} \\ t_1 - t'_1 & t_3 - t'_3 \end{bmatrix}^\top \begin{bmatrix} R_{11} \\ R_{13} \\ T_1 \\ R_{21} \\ R_{23} \\ T_2 \\ R_{31} \\ R_{33} \\ T_3 \\ 1 \end{bmatrix} = 0 \quad (8)$$

Since each frame provides two rows of \mathbf{A} , at least five frames captured in different poses are required to obtain a proper solution. Equation (8) can be modified into (9) or (10) using (4) if the line is parallel to x- or z-axis of the world coordinate system, respectively.

$$[\hat{\mathbf{v}}_y - \hat{\mathbf{v}}'_y \ \hat{\mathbf{v}}_z - \hat{\mathbf{v}}'_z]^\top \mathbf{x} = 0 \quad (9)$$

$$[\hat{\mathbf{v}}_x - \hat{\mathbf{v}}'_x \ \hat{\mathbf{v}}_y - \hat{\mathbf{v}}'_y]^\top \mathbf{x} = 0 \quad (10)$$

Accumulating rows of Matrix \mathbf{A} from multiple frames, a singular vector of \mathbf{A} , corresponding to its minimum singular value, is selected as an initial solution of the relative pose

$[\mathbf{R}_{LC} \ \mathbf{t}_{LC}]$. The second column of \mathbf{R}_{LC} , which is not included in the unknown vector \mathbf{x} , is computed by cross product of the third column and the first column of \mathbf{R}_{LC} . The orthonormal constraint of \mathbf{R}_{LC} is achieved by minimizing the Frobenius norm.

IV. NON-LINEAR OPTIMIZATION

A. Optimization Using a Plane

We assumed that the plane on which the scanned points lie is perpendicular to one of the axes of the world coordinate system. In most real cases, however, this assumption is not perfectly satisfied. An actual pose of the plane is included in an optimization process which will be explained in this section.

Let us assume that a plane is perpendicular to the y-axis of the world coordinate system, as in Sect. III-A. A normal vector of the plane is modelled as $\mathbf{n} = [n_1 \ 1 \ n_2]^\top$ (not a unit vector) because the plane is nearly perpendicular to the y-axis. The initial values of n_1 and n_2 are set to zero. An initial value of the constant term K of the plane is set to equal the y-coordinate of $\mathbf{q}'_W = \mathbf{H}\mathbf{q}'_L$, where \mathbf{q}'_L is the point selected in Sect. III-A.

The cost function f_P , of the non-linear optimization in this case, is defined as a squared sum of distances between the plane and scanned points in the world coordinate system.

$$f_P = \sum \left(\frac{\mathbf{n}^\top (\mathbf{H}\mathbf{q}_L) - K}{\|\mathbf{n}\|} \right)^2 \quad (11)$$

If the plane is perpendicular to the x- or z-axis of the world coordinate system, the cost function is the same as in (11), except for a normal vector of the plane modelled as $\mathbf{n} = [1 \ n_1 \ n_2]^\top$ or $\mathbf{n} = [n_1 \ n_2 \ 1]^\top$, respectively. As you may guess, an initial value of K is set to the x- or z-coordinate of \mathbf{q}'_W .

B. Optimization Using an Intersecting Line

In this section, we present two cost functions of non-linear optimization using an intersecting line. In the first one, a line is modelled by a starting point and a vector (not a unit vector). Let us assume that a line is parallel to y-axis of the world coordinate system, as in Sect. III-B. In this case, any point on the line can be expressed by (12).

$$\mathbf{p} + \lambda \mathbf{d} = \begin{bmatrix} K_1 \\ 0 \\ K_2 \end{bmatrix} + \lambda \begin{bmatrix} d_1 \\ 1 \\ d_2 \end{bmatrix} \quad (12)$$

The initial values of d_1 and d_2 are set to zero, and those of K_1 and K_2 are set to equal the x- and z-coordinates of $\hat{\mathbf{q}}'_W = \mathbf{H}\hat{\mathbf{q}}'_L$, respectively, where $\hat{\mathbf{q}}'_L$ is a feature point of the frame selected in Sect. III-B.

A cost function f_L of the non-linear optimization, in the case of using an intersecting line, is defined as a squared sum of distances between the line and feature points in the world coordinate system. Distances are measured in an x-z plane to simplify implementation. For each feature point, an unknown

scale λ is set to \hat{y}_W , the y-coordinate of $\hat{\mathbf{q}}_W = \mathbf{H}\hat{\mathbf{q}}_L$, to make the y-error equal to zero.

$$f_L = \sum \|\mathbf{p} + \lambda \mathbf{d} - (\mathbf{H}\hat{\mathbf{q}}_L)\|^2 \quad (13)$$

If the line is parallel to the x- or z-axis of the world coordinate system, (12) is changed into (14) or (15), and λ is set to the x- or z-coordinate of $\hat{\mathbf{q}}_W$ for each feature point, respectively. As you may guess, the initial values of K_1 and K_2 are set to equal the y- and z-coordinates, or x- and y-coordinates of $\hat{\mathbf{q}}'_W$, respectively.

$$\mathbf{p} + \lambda \mathbf{d} = \begin{bmatrix} 0 \\ K_1 \\ K_2 \end{bmatrix} + \lambda \begin{bmatrix} 1 \\ d_1 \\ d_2 \end{bmatrix} \quad (14)$$

$$\mathbf{p} + \lambda \mathbf{d} = \begin{bmatrix} K_1 \\ K_2 \\ 0 \end{bmatrix} + \lambda \begin{bmatrix} d_1 \\ d_2 \\ 1 \end{bmatrix} \quad (15)$$

The second cost-function of optimization utilizes all the scan data instead of feature points only. As mentioned above, an intersecting line is formed by two non-parallel planes. For this function, we minimized distances between the planes and scanned the data on them. Initial values of their normal vectors were computed by a cross product of line segments extracted from the selected frame in Sect. III-B, and an axis to which the intersecting line is parallel. Let us assume that the intersecting line is parallel to the y-axis, as in Sect. III-B. Let \mathbf{q}'_{LS} and \mathbf{q}'_{LE} be the start and end points of the scan data selected in Sect. III-B. The initial values of the normal vectors \mathbf{u}_1 , \mathbf{u}_2 were computed by (16) and (17), respectively.

$$\mathbf{u}_1 = (\mathbf{H}\hat{\mathbf{q}}'_L - \mathbf{H}\mathbf{q}'_{LS}) \times [0 \ 1 \ 0]^\top \quad (16)$$

$$\mathbf{u}_2 = (\mathbf{H}\hat{\mathbf{q}}'_L - \mathbf{H}\mathbf{q}'_{LE}) \times [0 \ 1 \ 0]^\top \quad (17)$$

Constant terms of the planes L_1 , L_2 were computed using the feature point $\hat{\mathbf{q}}'_L$ of the selected frame.

$$L_1 = \mathbf{u}_1^\top (\mathbf{H}\hat{\mathbf{q}}'_L) \quad (18)$$

$$L_2 = \mathbf{u}_2^\top (\mathbf{H}\hat{\mathbf{q}}'_L) \quad (19)$$

Let π_1 and π_2 be the planes with normal vectors \mathbf{u}_1 and \mathbf{u}_2 and constant terms L_1 and L_2 , respectively. A cost function f_2 is defined as a squared sum of distances between the planes and scan data in the world coordinate system.

$$f_2 = \sum_{\mathbf{q} \in \pi_1} \left(\frac{\mathbf{u}_1^\top (\mathbf{H}\mathbf{q}) - L_1}{\|\mathbf{u}_1\|} \right)^2 + \sum_{\mathbf{q} \in \pi_2} \left(\frac{\mathbf{u}_2^\top (\mathbf{H}\mathbf{q}) - L_2}{\|\mathbf{u}_2\|} \right)^2 \quad (20)$$

If the line is parallel to the x- or z-axis of the world coordinate system, the vector $[0 \ 1 \ 0]^\top$ in (16) and (17) is changed to $[1 \ 0 \ 0]^\top$ or $[0 \ 0 \ 1]^\top$, respectively.

V. EXPERIMENTAL RESULTS

A. Simulation using Synthetic Data

We performed an experiment using synthetic data to verify the accuracy of the proposed methods. First, we generated a random relative pose $[\mathbf{R}_{LC} \ \mathbf{t}_{LC}]$ between a camera and a 2D laser sensor. Then we generated a number of relative poses $[\mathbf{R}_{CW} \ \mathbf{t}_{CW}]$ between the camera and a world coordinate system. For each pose, we computed proper range data (i.e., angle-distance pair). In this simulation, we used ‘radians’ and ‘meters’ as measurement units of rotation and translation, respectively. Elements of rotation and translation of the relative poses were generated in intervals of $(-0.3, 0.3)$ and $(-0.5, 0.5)$, respectively. Rotation elements indicate a unit-normal vector of the rotation axis, multiplied by a rotation angle. In the case of using a plane, an unknown constant K is generated in $(1.0, 2.0)$, while in the case of using a line, the unknown constants K_1 and K_2 are generated far from the origin: $(2.0, 3.0)$ meters away from it.

In every experiment, we added Gaussian noise to the range data. Its mean was fixed at zero, and its standard deviation changed from 0 to 0.05. The translation vectors and range data were similar to real data measured in meters, and the noise of the real-range data was similar to $N(0, 10)$ in millimeters. In our simulation, a standard deviation of 0.05 was equivalent to that of 50 mm in real data (i.e., five times larger than actual noise). Simulation results are shown in Fig. 4. We also tried adding noise to structures but the results are not displayed because they showed almost no change from the noiseless cases. An error is measured by multiplying the final solution of $[\mathbf{R}_{LC} \ \mathbf{t}_{LC}]$ to an inverse of the ground-truth. Its rotation part was transformed into a Rodrigues form and its rotation angle (in radians) was picked as the rotation error. A Euclidean length of its translation part was picked as the translation error. Fig. 4 shows simulation results using the proposed methods. ‘Plane’ is the result using a plane (see Sect. III-A and IV-A), and ‘Line’ and ‘2 Planes’ are those using an intersecting line (see Sect. III-B and IV-B). For the optimization processes, only features were used for ‘Line’ while all points were used for ‘2 Planes’. ‘Conventional’ indicates results of the conventional method [24]. The results generated by using two planes were the best among the three newly proposed methods, and the conventional method.

The simulation results mentioned above assume that the camera-to-world transformations contain no error. In real cases, however, they are affected by the camera-calibration result. We added noise to intrinsic parameters of a camera and estimated the relative pose between the camera and a 2D laser sensor using both the conventional and the proposed methods. The standard deviations of the noise added to the range data, and of feature locations on images, were fixed to 10 mm and 0.5 pixels, respectively. The results are shown in Fig. 5.

We tried another experiment varying a range of camera-to-world transformation. The objective of this experiment was to determine camera-pose variations which are predominant and thus influence the accuracy of the final results. One of

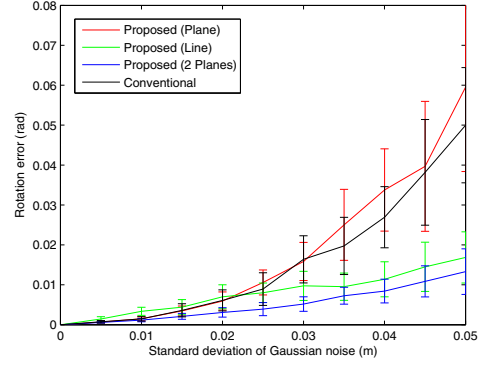


Fig. 4. Simulation results with a Gaussian noise in the range data: ‘Plane’ was computed using a plane while ‘Line’ and ‘2 Planes’ were computed using an intersecting line. ‘Line’ used line features only in an optimization process, while ‘2 Planes’ used all of the scan data. ‘Conventional’ was computed using the conventional method [24]. The proposed method using an intersecting line and all data for an optimization (2 Planes), performed best among all the methods. The error distribution was almost unchanged by the structure noise because it was reduced in an optimization process.

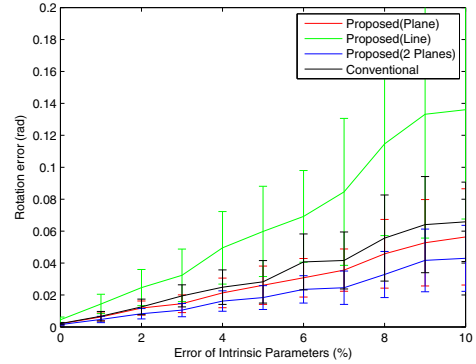


Fig. 5. The accuracy of the intrinsic parameters of a camera affects that of the relative pose between a 2D laser and the camera. In this graph, the standard deviations of the noises added to range data and feature location on images were fixed to 10 mm and 0.5 pixels, respectively.

three rotation parameters was generated in a wider interval than the other two. In the case of using a plane perpendicular to the y-axis (see Fig. 6), the rotation on the x-axis and translation on the y-axis, were important for the accuracy of the results. In the case of using an intersecting line parallel to the y-axis (see Fig. 7), the result was not seriously affected by any dimension of the camera-to-world transformation. In both Fig. 6 and 7, numbers indicate the intervals at which parameters were generated: for example, ‘Rx 0.5, Ry 0.2, Rz 0.2’ means that Rx was generated in $(-0.5, 0.5)$ while Ry and Rz were generated in $(-0.2, 0.2)$. These experiments clearly show that the relative pose between camera and laser is hardly constrained by movements with a small change of structure, in the sensor coordinate system. That is why a lot of data must be captured in various poses, especially those which change the structures greatly.

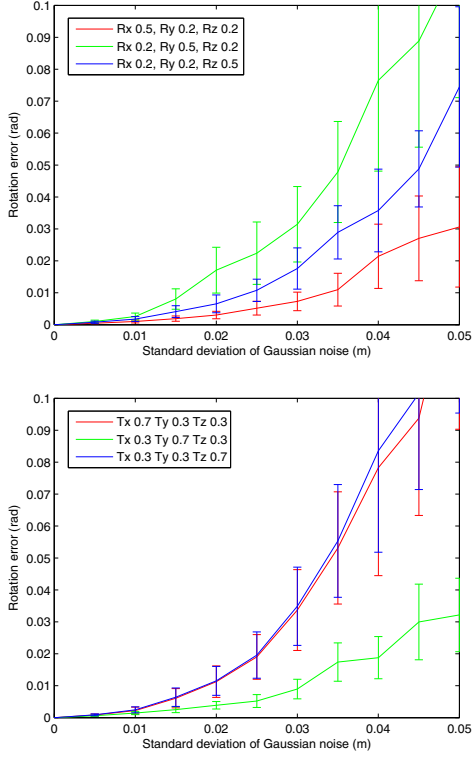
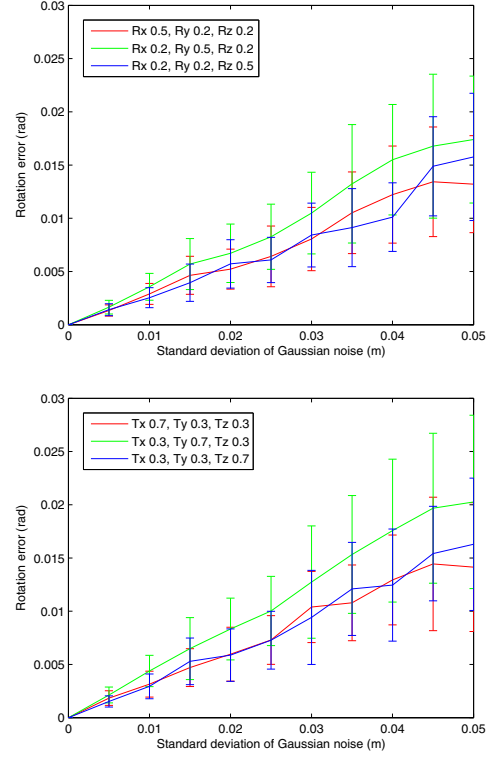


Fig. 6. These figures show which element of the camera-to-world transformation is critical to the accuracy of the final result, when using a plane perpendicular to the y-axis of the world coordinate system. Rotation on the x-axis (i.e., the pitch of a laser sensor) and translation on the y-axis (i.e., distance variation from laser to plane) were important for obtaining good results.

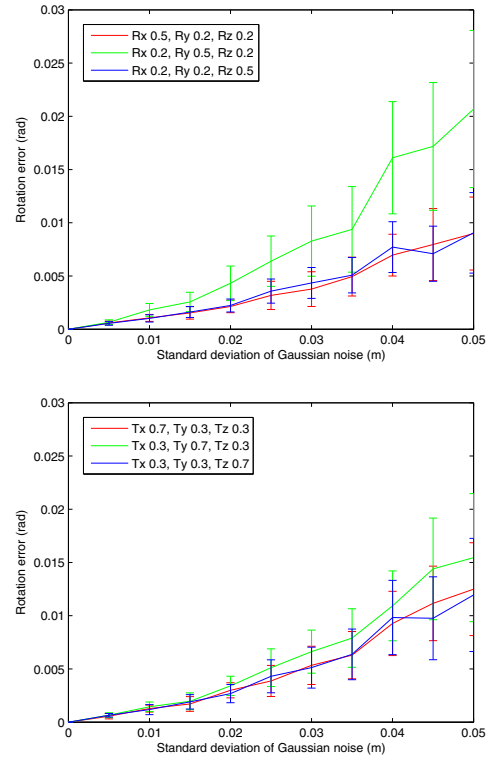
B. Experiments using Real Data

We also performed experiments using real data. We built a system consisting of two cameras (PointGrey Flea2 with 3.5mm lens), and a 2D laser sensor (Hokuyo UTM- 30LX). The heading directions of the cameras were perpendicular, and the laser sensor was parallel to one camera to ensure that the other camera could not see the scan data (see Fig. 8). The system was fully calibrated: camera calibration by Z. Zhang [27] and camera-laser calibration by Zhang and Pless [24]. A relative pose between two non-overlapping cameras was also computed by solving the $AX=XB$ problem [28]. The environment, including a pattern plane captured for experiments, is shown in Fig. 9.

Combination of Camera 1 and the laser sensor in Fig. 8 can be calibrated both by the conventional method [24] and by the proposed methods because the angular range of the laser sensor is wide enough (270 degrees) to contain both overlapping and non-overlapping areas. Its 45-degree direction was parallel to the heading direction of Camera 1. We utilized a part of the scan data between 0 and 90 degrees for the conventional method, and the other data for the proposed methods. Since we do not know the ground-truth of the calibration results, we ‘measured’ distances among the sensors manually using a ruler. The calibration results are shown in Table I. ‘Line’ and ‘2 Planes’ results were



(a) Result using only features for optimization



(b) Result using all data for optimization

Fig. 7. These figures show which element of the camera-to-world transformation was critical to the accuracy of a final result, using an intersecting line parallel to the y-axis of the world coordinate system. Unlike in Fig. 6, this result is robust and not seriously affected by any dimension of the camera-to-world transformation. In all cases, rotation/translation on an intersecting line (parallel to the y-axis in this case) has a relatively small influence on the accuracy of the result.

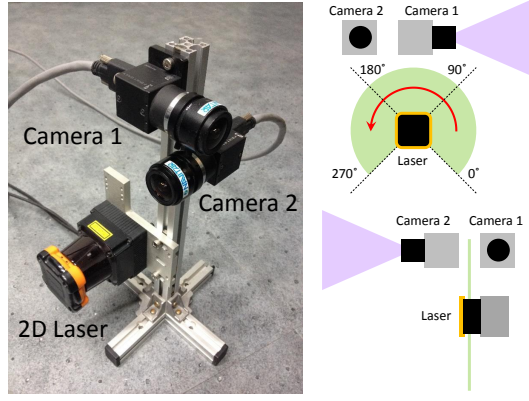


Fig. 8. Sensor system to capture non-overlapping calibration data

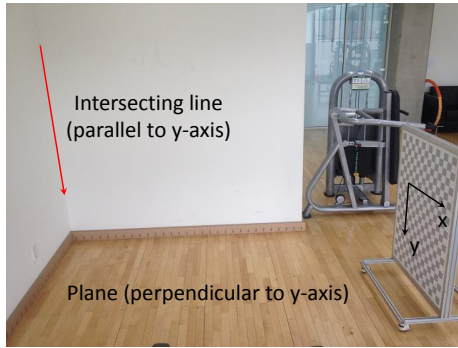


Fig. 9. Experimental environment containing a planar pattern and two white planes whose intersecting line is parallel to the y-axis of the world coordinate system.

obtained by the first and the second methods, respectively, of Sect. IV-B, with an initial value from Sect. III-B. In this experiment, we utilized two planes perpendicular to the x- and z-axis of the world coordinate system (i.e., the line of their intersection is parallel to the y-axis). This means that we can also apply the proposed method using a plane. ‘Plane 1’ and ‘Plane 2’ results were obtained by the method of Sect. IV-A, with an initial value from Sect. III-A.

The combination of Camera 2 and the laser sensor in Fig. 8 cannot be calibrated by the conventional method because there is no overlap between their fields of view. It can only be calibrated indirectly using Camera 1 as a ‘bridging’ device, by multiplying a relative pose between two cameras, with that between Camera 1 and the laser sensor. The proposed

TABLE I
ESTIMATED RELATIVE POSE (TRANSLATION) BETWEEN CAMERA 1 AND LASER SENSOR

	Translation (mm)		
Measured	208	-48	-92
Conventional [24]	206.436	-26.345	-83.356
Proposed (Line)	214.164	-58.081	-91.103
Proposed (2 Planes)	214.088	-58.206	-89.525
Proposed (Plane 1)	212.189	-14.837	-89.738
Proposed (Plane 2)	207.530	-41.153	-104.668

TABLE II
ESTIMATED RELATIVE POSE (TRANSLATION) BETWEEN CAMERA 2 AND LASER SENSOR

	Translation (mm)		
Measured	-168	74	30
Conventional [24]	-166.331	66.063	6.874
Proposed (Line)	-169.889	75.676	6.598
Proposed (2 Planes)	-170.865	73.360	34.503
Proposed (Plane 1)	-164.658	74.018	30.102
Proposed (Plane 2)	-171.759	68.960	3.174

TABLE III
ESTIMATED RELATIVE POSE (TRANSLATION) BETWEEN CAMERA 1 AND LASER SENSOR

	Translation (mm)		
Measured	-168	74	30
Conventional [24]	-166.331	66.063	6.874
Proposed (Plane)	-167.183	71.487	6.424

methods were applied to this combination directly without any bridging device. The laser sensor scanned an intersecting line of a floor and a vertical wall while Camera 2 captured images of a vertical planar pattern. In this case, the two planes were perpendicular to the x and y axes of the world coordinate system (i.e., their line of intersection was parallel to the z-axis). Results are shown in Table II. The proposed methods were explained in the previous paragraph, and the conventional method used the multiplied result mentioned above.

The results in both Table I and II show that the proposed method using an intersecting line and two-plane optimization, provided stable results. The results using a plane are sometimes more accurate than those using an intersecting line, but their accuracy depends on the datasets because the plane-based method often converges to a local minimum. We recommend to utilize at least two planes for camera-laser calibration.

We also tried another experiment. The conventional method uses a planar pattern which is identical to that observed by a camera. We applied our plane-based method with a plane perpendicular to the z-axis (i.e., parallel to the planar pattern) and compared its accuracy to that of the conventional method. The results are shown in Table III. Although the proposed method has additional unknown variables (i.e., pose of the plane), the results achieved by the two methods were similar.

VI. CONCLUSION

We proposed solutions to achieve an extrinsic calibration of a camera and a 2D laser without overlap. We utilized a planar pattern and one of two types of artificial structures: a plane or an intersecting line of two planes. In each case, an initial solution of the relative pose between sensors was estimated easily using singular value decomposition. Then the solution was refined via non-linear optimization, which

minimizes the Euclidean distance between structures and scan data.

To our knowledge, this paper is the first attempt to achieve extrinsic calibration of non-overlapping camera-laser systems. Simple equations based on reasonable assumptions and simulation results, showed the effectiveness of the proposed methods. Experiments using real data also provided reliable results similar to those measured by ruler.

However, we still have the problem of local minima in the plane-based methods. It seems more unreliable than we observed in simulation. We are looking for problems in the real data that might make the results of the plane-based methods unstable.

VII. ACKNOWLEDGMENTS

This research is supported by the National Research Foundation, Korea, under the NRF-ANR joint research programme (No. 2011-0031920).

REFERENCES

- [1] N. Snavely, S. M. Seitz and R. Szeliski, "Photo tourism: Exploring photo collections in 3D," *ACM Transactions on Graphics (Proc. ACM SIGGRAPH)*, vol. 25, no. 3, pp. 835-846, 2006.
- [2] M. Pollefeys, D. Nistér, J.-M. Frahm, A. Akbarzadeh, P. Mordohai, B. Clipp, C. Engels, D. Gallup, S.-J. Kim, P. Merrell, C. Salmi, S. Sinha, B. Taiton, L. Wang, Q. Yang, H. Stewénus, R. Yang, G. Welch and H. Towles, "Detailed Real-Time Urban 3D Reconstruction from Video," *International Journal of Computer Vision*, vol. 78, no.2-3, pp. 143-167, 2008.
- [3] A. J. Davison, I. D. Reid, N. D. Molton and O. Stasse, "MonoSLAM: Real-Time Single Camera SLAM," *IEEE Transactions on Pattern Analysis and Machine Intelligence*, vol. 29, no. 6, pp. 1052-1067, 2007.
- [4] S. Thrun, "Robotic Mapping: A Survey," in *Exploring Artificial Intelligence in the New Millennium*, Morgan Kaufmann Publishers, 2003, pp. 1-35.
- [5] A. Howard, D. F. Wolf and G. S. Sukhatme, "Towards 3D Mapping in Large Urban Environments," in *Proceedings of the IEEE/RSJ International Conference on Intelligent Robots and Systems*, 2004, pp.419-424.
- [6] C. Frueh, S. Jain and A. Zakhori, "Data Processing Algorithms for Generating Textured 3D Building Façade Meshes from Laser Scans and Camera Images," *International Journal of Computer Vision*, vol. 61, no. 2, pp. 159-184, 2005.
- [7] P. Pfaff et al., "Towards Mapping of Cities," in *Proceedings of the IEEE International Conference on Robotics and Automation*, 2007, pp. 4807-4813.
- [8] A. Banno, T. Masuda, T. Oishi and K. Ikeuchi, "Flying Laser Range Sensor for Large-Scale Site-Modeling and Its Applications in Bayon Digital Archival Project," *International Journal of Computer Vision*, vol. 78, no.2-3, pp. 207-222, 2008.
- [9] R. C. Luo, C. C. Lai and C. C. Hsiao, "Enriched Indoor Environment Map Building Using Multi-Sensor Based Fusion Approach," in *Proceedings of the IEEE/RSJ International Conference on Intelligent Robots and Systems*, 2010, pp. 2059-2064.
- [10] G. Gallegos and P. Rives, "Indoor SLAM Based on Composite Sensor Mixing Laser Scans and Omnidirectional Images," in *Proceedings of the IEEE International Conference on Robotics and Automation*, 2010, pp. 3519-3524.
- [11] X. Zhang, A. B. Rad and Y.-K. Wong, "Sensor Fusion of Monocular Cameras and Laser Rangefinders for Line-Based Simultaneous Localization and Mapping (SLAM) Tasks in Autonomous Mobile Robots," *Sensors*, vol. 12, no. 1, pp. 429-452, 2012.
- [12] P. Biber, H. Andreasson, T. Duckett and A. Schilling, "3D Modeling of Indoor Environments by a Mobile Robot with a Laser Scanner and Panoramic Camera," in *Proceedings of the IEEE/RSJ International Conference on Intelligent Robots and Systems*, 2004, pp. 3430-3435.
- [13] Y. Bok, Y. Jeong, D.-G. Choi and I. S. Kweon, "Capturing Village-level Heritages with a Hand-held Camera-Laser Fusion Sensor," *International Journal of Computer Vision*, vol. 94, no. 1, pp. 36-53, 2011.
- [14] R. A. Newcombe, S. Izadi, O. Hilliges, D. Molyneaux, D. Kim, A. J. Davison, P. Kohli, J. Shotton, S. Hodges and A. Fitzgibbon, "KinectFusion: Real-time Dense Surface Mapping and Tracking," in *Proceedings of the IEEE International Symposium on Mixed and Augmented Reality*, 2011, pp. 127-136.
- [15] S. A. Scherer, D. Dube and A. Zell, "Using Depth in Visual Simultaneous Localisation and Mapping," in *Proceedings of the IEEE International Conference on Robotics and Automation*, 2012, pp. 5216-5221.
- [16] T. Whelan, H. Johannsson, M. Kaess, J. J. Leonard and J. McDonald, "Robust Real-Time Visual Odometry for Dense RGB-D Mapping," in *Proceedings of the IEEE International Conference on Robotics and Automation*, 2013, pp. 5704-5711.
- [17] Q. Zhang, M. Ye, R. Yang, Y. Matsushita, B. Wilburn and H. Yu, "Edge-Preserving Photometric Stereo via Depth Fusion," in *Proceedings of the IEEE Conference on Computer Vision and Pattern Recognition*, 2012, pp. 2472-2479.
- [18] J. T. Barron and J. Malik, "Intrinsic Scene Properties from a Single RGB-D Image," in *Proceedings of the IEEE Conference on Computer Vision and Pattern Recognition*, 2013, pp. 17-24.
- [19] L.-F. Yu, S.-K. Yeung, Y.-W. Tai and S. Lin, "Shading-based Shape Refinement of RGB-D Images," in *Proceedings of the IEEE Conference on Computer Vision and Pattern Recognition*, 2013, pp.1415-1422.
- [20] R. K. Kumar, A. Ilie, J.-M. Frahm and M. Pollefeys, "Simple Calibration of Non-overlapping Cameras with a Mirror," in *Proceedings of the IEEE Conference on Computer Vision and Pattern Recognition*, 2008, pp. 1-7.
- [21] P. L  braly, E. Royer, O. Ait-Aider, C. Deymier and M. Dhome, "Fast Calibration of Embedded Non-Overlapping Cameras," in *Proceedings of the IEEE International Conference on Robotics and Automation*, 2011, pp. 221-227.
- [22] D. Scaramuzza, A. Harati and R. Siegwart, "Extrinsic Self Calibration of a Camera and a 3D Laser Range Finder from Natural Scenes," in *Proceedings of the IEEE/RSJ International Conference on Intelligent Robots and Systems*, 2007, pp. 4164-4169.
- [23] J. Jung, Y. Jeong, J. Park, H. Ha, J. D. Kim and I.-S. Kweon, "A Novel 2.5D Pattern for Extrinsic Calibration of ToF and Camera Fusion System," in *Proceedings of the IEEE/RSJ International Conference on Intelligent Robots and Systems*, 2011, pp. 3290-3296.
- [24] Q. Zhang and R. Pless, "Extrinsic Calibration of a Camera and Laser Range Finder (improves camera calibration)," in *Proceedings of the IEEE/RSJ International Conference on Intelligent Robots and Systems*, 2004, pp. 2301-2306.
- [25] C. Mei and P. Rives, "Calibration between a Central Catadioptric Camera and a Laser Range Finder for Robotic Applications," in *Proceedings of the IEEE International Conference on Robotics and Automation*, 2006, pp. 532-537.
- [26] G. Li, Y. Liu, L. Dong, X. Cai and D. Zhou, "An Algorithm for Extrinsic Parameters Calibration of a Camera and a Laser Range Finder Using Line Features," in *Proceedings of the IEEE/RSJ International Conference on Intelligent Robots and Systems*, 2007, pp. 3854-3859.
- [27] Z. Zhang, "A Flexible New Technique for Camera Calibration," *IEEE Transactions on Pattern Analysis and Machine Intelligence*, vol. 22, no. 11, pp. 1330-1334, 2000.
- [28] F. C. Park and B. J. Martin, "Robot Sensor Calibration: Solving $AX=XB$ on the Euclidean Group," *IEEE Transactions on Robotics and Automation*, vol. 10, no. 4, pp. 717-721, 1994.
- [29] D.-G. Choi, Y. Bok, J.-S. Kim and I. S. Kweon, "Extrinsic Calibration of 2D Laser Sensors," in *Proceedings of the IEEE International Conference on Robotics and Automation*, 2014, pp. 3027-3033.